

Fluid-Particle Drag in Inertial Polydisperse Gas–Solid Suspensions

William Holloway, Xiaolong Yin, and Sankaran Sundaresan
 Dept. of Chemical Engineering, Princeton University, Princeton, NJ 08544

DOI 10.1002/aic.12127

Published online December 22, 2009 in Wiley InterScience (www.interscience.wiley.com).

In this article, we extend the low Reynolds number fluid-particle drag relation proposed by Yin and Sundaresan for polydisperse systems to include the effect of moderate fluid inertia. The proposed model captures the fluid-particle drag results obtained from lattice-Boltzmann simulations of bidisperse and ternary suspensions at particle mixture Reynolds numbers ranging from $0 \leq Re_{mix} \leq 40$, over a particle volume fraction range of $0.2 \leq \phi \leq 0.4$, volume fraction ratios of $1 \leq \phi_i/\phi_j \leq 3$, and particle diameter ratios of $1 \leq d_i/d_j \leq 2.5$. © 2009 American Institute of Chemical Engineers AICHE J, 56: 1995–2004, 2010

Keywords: fluid-particle drag force, polydisperse mixtures, lattice-Boltzmann simulation, multi-fluid model, moderate inertia, fluidized bed

Introduction

Analysis of large scale gas-particle flows, which are widely encountered in the chemical process industry, is commonly done using averaged equations of motion where the individual particle phase(s) and the fluid are treated as interpenetrating continua.^{1–3} These equations contain several terms—the fluid-particle drag force, the particle and fluid-phase effective stresses, etc.—which require constitutive relations. Among these, the fluid-particle drag plays a dominant role in gas–solid fluidized beds in balancing the gravitational force acting on the particles.^{2–8} A number of constitutive relations for the fluid-particle drag in monodisperse suspensions (i.e., particles of the same size/density) can be found in the literature.^{1–3,9–14} Polydispersity (differences in particle size and/or density) is common in most industrial scale devices; addition of fines is known to affect the quality of fluidization,¹⁵ and segregation is an important consideration in polydisperse fluidized beds.^{16–18} Indeed, a substantial amount of recent research has been devoted to the formulation of fluid-particle drag relations for polydisperse fixed beds and suspensions (for example see following references, and the references cited therein).^{7,8,12,19} Beetstra et al.¹⁹ provide expressions for fluid-particle drag in polydisperse fixed

beds over a range of Reynolds numbers, while Yin and Sundaresan^{7,8} limit themselves to Stokes flow conditions, but allow for relative motion (in the local average sense) between the various types of particles.

This study builds on the earlier studies by Yin and Sundaresan^{7,8} and considers the effect of moderate inertia on the fluid-particle drag in polydisperse systems, allowing for relative motion between the different types of particles. Towards this end, we have carried out lattice-Boltzmann simulations of fluid flow through assemblies of polydisperse particles in periodic domains, and extracted the fluid-particle drag force under conditions where fluid inertia has a non-negligible effect. We find that the results can be captured reasonably well by a new drag force model for polydisperse suspensions that combines the expressions proposed by Yin and Sundaresan^{7,8} for Stokes flow of suspensions and the inertial correction developed by Beetstra et al.¹⁹ for monodisperse fixed beds. We restrict our attention to large Stokes number and moderate Reynolds numbers based on the local-average slip velocity between the fluid and the different types of particles; these conditions are indeed satisfied by most gas-fluidized beds. Strictly speaking, the fluid-particle drag force will also depend on the Reynolds number based on the fluctuating velocities of the particles²⁰; however, in fluidized suspensions, the fluctuating velocities of the particles tend to be considerably smaller than the local-average fluid-particle slip velocity, and so their effect on the drag force is only weak.²⁰ With this in mind, we have not engaged in a

Correspondence concerning this article should be addressed to S. Sundaresan at sundar@princeton.edu.

systematic study of the effect of particle velocity fluctuations on the fluid particle drag in polydisperse systems.

This article is organized as follows: we first present the fluid-particle drag relations proposed by Beetstra et al.¹⁹ for polydisperse fixed beds and Yin and Sundaresan^{7,8} for polydisperse suspensions under Stokes flow conditions, and propose an extension of the Yin and Sundaresan^{7,8} expressions to account for the effect of moderate fluid inertia. We then outline the lattice-Boltzmann simulation procedure and present the results for polydisperse suspensions with relative motion between the different particle types at moderate fluid inertia. These simulation results are then used to validate the proposed drag force model. The article then concludes with a summary of the main results.

Fluid-Particle Interaction Force in Polydisperse Systems

Fixed beds

The total fluid-particle interaction force per unit volume of a polydisperse *fixed* bed acting on particle of type i , $\mathbf{f}_{\text{Di-fixed}}$, is usually expressed as

$$\mathbf{f}_{i\text{-fixed}} = -\phi_i \nabla P + \mathbf{f}_{\text{Di-fixed}}; \quad \mathbf{f}_{\text{Di-fixed}} = -\beta_i \Delta \mathbf{U} \quad (1)$$

where P is the local-average fluid pressure, ϕ_i is the volume fraction of particles of type i , $\mathbf{f}_{\text{Di-fixed}}$ is the fluid-particle drag force *per unit volume* of the bed, β_i is the volume-specific friction coefficient for particles of type i , and $\Delta \mathbf{U}$ is the difference between the local average velocities of the particle and fluid phases. It is convenient to express the fixed-bed friction coefficient β_i as^{7,8,12,19}

$$\beta_i = \frac{18\phi_i(1-\phi)\mu}{d_i^2} F_{\text{Di-fixed}}^* \quad (2)$$

where ϕ is the total particle phase volume fraction, d_i is the diameter of the i th particle species, μ is the fluid viscosity; $F_{\text{Di-fixed}}^*$ is a dimensionless fluid-particle drag on a particle of type i in a polydisperse fixed bed ($F_{\text{Di-fixed}}^*$ is nondimensionalized by the Stokes drag, namely $3\pi\mu d_i(1-\phi)\Delta U$). Yin and Sundaresan⁸ recently proposed the following expression for $F_{\text{Di-fixed}}^*$ for Stokes flow through polydisperse fixed beds (particle diameter ratios up to 4:1):

$$F_{\text{Di-fixed}}^* = \left(\frac{1}{1-\phi} \right) + \left(F_{\text{D-fixed}}^* - \frac{1}{1-\phi} \right) (ay_i + (1-a)y_i^2) \quad (3)$$

where $y_i = d_i/\langle d \rangle$; $\langle d \rangle$ is the Sauter mean diameter

$$\langle d \rangle = \frac{\sum_i n_i d_i^3}{\sum_i n_i d_i^2}; \quad (4)$$

$F_{\text{D-fixed}}^*$ is the dimensionless fluid particle drag force in a monodisperse fixed bed¹²

$$F_{\text{D-fixed}}^* = \frac{10\phi}{(1-\phi)^2} + (1-\phi)^2 (1 + 1.5\sqrt{\phi}) \quad (5)$$

and a is a cubic polynomial of volume fraction:

$$a = 1 - 2.66\phi + 9.096\phi^2 - 11.338\phi^3. \quad (6)$$

To account for the effects of moderate fluid inertia on the monodisperse fixed bed drag force, Beetstra et al.¹⁹ modified Eq. 5 as

$$F_{\text{D-fixed}}^* = \left(\frac{10\phi}{(1-\phi)^2} + (1-\phi)^2 (1 + 1.5\sqrt{\phi}) \right) (1 + \chi_{\text{BVK}}). \quad (7)$$

where χ_{BVK} represents the inertial correction:

$$\chi_{\text{BVK}} = \frac{0.413\text{Re}}{240\phi + 24(1-\phi)^4(1 + 1.5\sqrt{\phi})} \times \frac{(1-\phi)^{-1} + 3\phi(1-\phi) + 8.4\text{Re}^{-0.343}}{1 + 10^3\phi\text{Re}^{\frac{-(1+4\phi)}{2}}}. \quad (8)$$

Here, Re is the Reynolds number, defined as follows

$$\text{Re} = \frac{|\Delta \mathbf{U}|(1-\phi)d}{\nu} \quad (9)$$

where ν is the fluid kinematic viscosity.

Polydisperse suspensions with particle-particle relative motion

Stokes Flow Regime. For high Stokes number, low Reynolds number suspensions with particle-particle relative motion, Yin and Sundaresan^{7,8} proposed the following drag force model:

$$\mathbf{f}_i = -\phi_i \nabla P + \mathbf{f}_{\text{Di}}; \quad \mathbf{f}_{\text{Di}} = -\beta_i \Delta \mathbf{U}_i - \sum_{j \neq i} \beta_{ij} (\Delta \mathbf{U}_j - \Delta \mathbf{U}_i) \quad (10)$$

For one-dimensional flow, the drag force expression can be written as

$$f_{\text{Di}}^* = -\beta_i^* \text{Re}_i - \sum_{j \neq i} \beta_{ij}^* \text{sgn}(\Delta U_j - \Delta U_i) \text{Re}_{ji}, \quad (11)$$

where, f_{Di}^* is the dimensionless fluid-particle drag force *per unit volume* suspension experienced by particles of type i ; $\beta_i^* = \frac{\rho_f \langle d \rangle^3}{\mu^2} \beta_i$ is the dimensionless fixed bed friction coefficient for particles of type i (with ρ_f denoting the fluid density and the dimensional friction coefficient β_i being given by Eqs. 2–6); $\beta_{ij}^* = \frac{\rho_f \langle d \rangle^3}{\mu^2} \beta_{ij}$ is the (dimensionless) fluid-mediated particle-particle drag friction coefficient; $\text{sgn}(\Delta U_j - \Delta U_i)$ is the signum function of $\Delta U_j - \Delta U_i$; Re_i and Re_{ji} are given as

$$\text{Re}_i = \frac{\langle d \rangle |\Delta U_i|}{\nu}, \quad \text{Re}_{ji} = \frac{\langle d \rangle |\Delta U_j - \Delta U_i|}{\nu}. \quad (12)$$

Note that the signum function is used in Eq. 11 to account for the change in sign of the fluid mediated particle-particle drag when the velocities of different particle types relative to one another change sign, while still retaining a positive definite form of Re_{ji} . For β_{ij}^* , Yin and Sundaresan⁸ proposed:

$$\beta_{ij}^* = -2\alpha_{ij} \frac{\phi_i \phi_j}{\frac{\phi_i}{\beta_i} + \frac{\phi_j}{\beta_j}} \quad (13)$$

where α_{ij} is a parameter that depends on the ratio of the lubrication cutoff distance λ (discussed later in this article) to the smaller particle diameter of i and j species:

$$\alpha_{ij} = 1.313 \log_{10} \left(\frac{\min(d_i, d_j)}{\lambda} \right) - 1.249. \quad (14)$$

Modification to Account for the Effect of Moderate Fluid Inertia. This study is concerned with extending the model proposed by Yin and Sundaresan⁸ for Stokes flow regime to account for moderate inertia. It will be demonstrated in this article that a simple modification, which includes the inertial correction for fixed beds proposed by Beetstra et al.,^{19,21} presented later, is able to capture drag force results extracted from our lattice-Boltzmann simulations. Specifically, the modified model consists of Eqs. 2–4, 6, 10, 12–14, and the following:

$$F_{D\text{-fixed}}^* = \left(\frac{10\phi}{(1-\phi)^2} + (1-\phi)^2 (1 + 1.5\sqrt{\phi}) \right) (1 + \chi_{\text{BVK}}^*) \quad (15)$$

where χ_{BVK}^* is given by:

$$\chi_{\text{BVK}}^* = \frac{0.413 \text{Re}_{\text{mix}}}{240\phi + 24(1-\phi)^4 (1 + 1.5\sqrt{\phi})} \times \frac{(1-\phi)^{-1} + 3\phi(1-\phi) + 8.4 \text{Re}_{\text{mix}}^{-0.343}}{1 + 10^3 \phi \text{Re}_{\text{mix}}^{-\frac{(1+4\phi)}{2}}}. \quad (16)$$

These two equations differ from Eqs. 7 and 8 slightly, with Re being replaced by Re_{mix} :

$$\text{Re}_{\text{mix}} = \frac{|\Delta U_{\text{mix}}| (1-\phi) \langle d \rangle}{\nu}; \quad \Delta U_{\text{mix}} = \frac{\sum_i \phi_i \Delta U_i}{\sum_i \phi_i}. \quad (17)$$

Effect of Particle Velocity Fluctuations. Strictly speaking, whenever fluid inertia plays a non-negligible role, the fluid-particle drag force is not independent of fluctuating particle motions.²⁰ For monodisperse suspensions, Wylie et al.²⁰ have modeled the effect of particle velocity fluctuations on the fluid-particle drag in a large-Stokes-number, moderate-Reynolds-number monodisperse suspension; toward this end, they define a Reynolds number based on particle velocity fluctuations as $\text{Re}_T = dT^{0.5}/\nu$ where the granular temperature $T = (1/3)(\langle(\Delta U)^2\rangle - \langle\Delta U\rangle^2)$ and the angle brackets indicate ensemble averages. They found that the effect of particle velocity fluctuations on the fluid-particle drag is very small provided Re_T is much smaller than the Reynolds number based on mean flow velocity and particle diameter (Re_m). Figure 1 illustrates the variation of the fluid-particle drag with particle velocity fluctuations scaled by the fluid-particle drag in the absence of particle velocity fluctuations plotted with Re_T/Re_m for $\text{Re}_m = 20$ and two different values of particle volume fractions, as given by the theory of Wylie

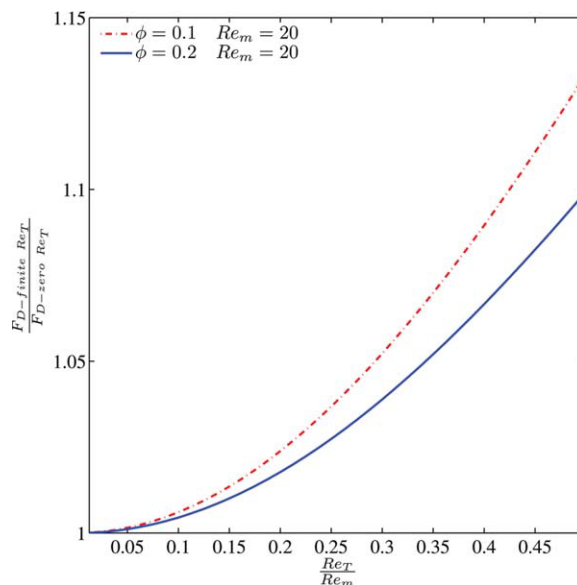


Figure 1. The effect of particle velocity fluctuations on the fluid-particle drag force in a suspension of uniformly sized spherical particles.

The Reynolds number associated with the mean slip velocity, $\text{Re}_m = 20$. Re_T refers to the Reynolds number associated with the particle velocity fluctuations. The ordinate shows the fluid-particle drag force in the presence of particle velocity fluctuations scaled with respect to that obtained in the absence of velocity fluctuations (i.e., a random fixed bed). The results are obtained using the model proposed by Wylie et al.²⁰ The two curves correspond to two different particle volume fractions. [Color figure can be viewed in the online issue, which is available at www.interscience.wiley.com.]

et al.²⁰ It is clear that when Re_T/Re_m is small the effect of particle velocity fluctuations on the fluid-particle drag is small. In Figure 2, we present results on the Re_m/Re_T ratio obtained from a lattice-Boltzmann simulation of a collection of bidisperse particles in a periodic domain, sedimenting freely under the action of gravity. (Details of the lattice-Boltzmann simulation methodology are discussed later.) The two curves correspond to the two types of particles in the mixture. It is clear that Re_m/Re_T is much larger than unity for both particle types. The results from the study by Wylie et al. for monodisperse systems (presented in Figure 1) then suggest that in polydisperse systems such as those occurring in gas-fluidized beds, the effect of particle velocity fluctuations on the fluid-particle drag is quite small. With this in mind, we have not explored the Re_T -dependence of fluid-particle drag in the present study.

Lattice-Boltzmann Simulations

To generate the computational data needed to develop and verify the fluid-particle drag force model, we simulated fluid flow through assemblies of particles using the lattice-Boltzmann scheme developed by Ladd,^{22–24} which has been used in a number of earlier studies.^{7,8,12,19,20,25,26} Ladd's code has been used by a number of investigators to study particle-laden flows, and we have used the same code. As details about the method are readily available in the literature, we

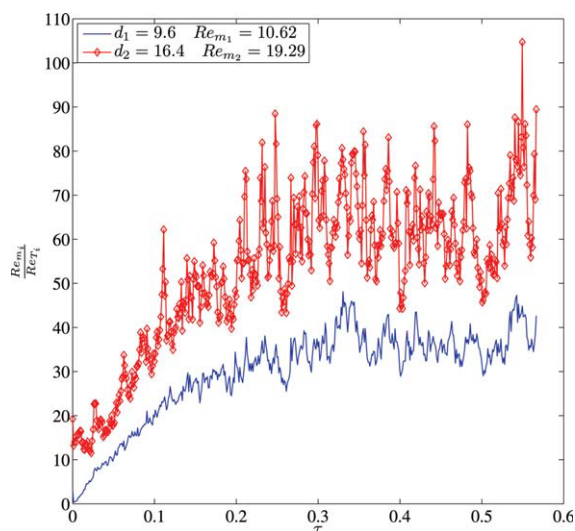


Figure 2. The evolution of Re_m/Re_t as a function of $\tau = tv/\langle d \rangle^2$ in a freely evolving, bidisperse, sedimenting, suspension, where t is time in lattice units, v is the fluid kinematic viscosity, and $\langle d \rangle$ is the Sauter mean diameter of the mixture.

The diameters of the two particles indicated in the figure are multiples of the lattice spacing. The Re_m values indicated in the figure are the statistical average values in the plateau region. The volume fraction of each particle type is the same. The collisions between the particles are elastic. The simulation was carried out in a cubic periodic box of dimension $L = 110$ lattice spacing, containing 144 Type 1 and 29 Type 2 particles. The particle density to fluid density ratio is 1000. $d_1 = 9.6$ and $d_2 = 16.4$, giving a total particle volume fraction of $\phi = 0.1$. A gravitational force $g\langle d \rangle^3/v^2 = 0.897$ is applied in the x -direction, and balanced by a pressure gradient equal to the weight of the suspension per unit volume. [Color figure can be viewed in the online issue, which is available at www.interscience.wiley.com.]

provide only a brief outline of the computational procedure. The 3-D lattice-Boltzmann method used in this study employs at 19-point quadrature in velocity space, the so-called D3Q19 model, with fluid density $\rho_f = 36$ (lattice units [l.u.]). To access a range of Re_m values, various fluid viscosity values ($\mu_f = 0.03$ and 0.36 [l.u.]) were used, while still maintaining low fluid velocities (<0.02 in [l.u.]) to ensure numerical stability. The particle sizes used in this study varied with the smallest particle diameter being ~ 10 lattice units. The effect of lattice resolution has been addressed by comparing and extrapolating simulation results obtained using different lattice resolutions.

When the separation between particles becomes smaller than the lattice spacing, the hydrodynamic (lubrication) interaction between the particles cannot be resolved in the simulations and are added explicitly.²⁷ For perfectly spherical, approaching particle pairs, the lubrication force would diverge near contact; in reality, such a divergence is removed by particle surface roughness, or non-continuum effects. To model this effect, it is implemented in the simulations that the lubrication force saturates at a value corresponding to a user specified separation known as the lubrication cut-off distance (λ). Yin and Sundaresan⁸ found that the

off-diagonal friction coefficient depended systematically on the value of λ (see Eqs. 13 and 14). In our simulations, we used a value of $\lambda = 0.01$ (l.u.) for our lattice-Boltzmann simulations performed at a fluid viscosity of $\mu_f = 0.36$ (l.u.). In our simulations performed at a fluid viscosity of $\mu_f = 0.03$ (l.u.), we assigned a value of λ so that every lattice resolution had an identical $\lambda/\min(d_i, d_j)$ ratio equal to 0.001.

Our simulations began by placing a binary mixture of spheres in a cubic periodic simulation domain whose sides are 10–15 times larger than the diameter of the smaller particle. A large number of Monte Carlo movements of these particles were then executed to ensure that the particle microstructure obeyed that of a binary hard sphere configuration.⁸ Subsequently, each particle type was assigned its desired (local average) velocity (ΔU_1 and ΔU_2); this induced fluid flow in the interstices of the particle assembly, whose evolution was followed via lattice-Boltzmann method. To ensure that the average fluid velocity approached zero, a pressure gradient was imposed on the fluid phase. This provides a means of specifying ΔU_1 and ΔU_2 before the simulation instead of extracting the values after the simulation by subtracting the resulting fluid velocity. Once a steady state was reached, the total fluid-particle interaction force F_i (ensemble averaged fluid-particle interaction force per particle) was obtained by integrating the traction due to the fluid over the surfaces of all the like particles. The fluid-particle drag was then isolated by removing the contribution due to the imposed pressure gradient (see Eq. 10). The number of particles used in each simulation varied depending on the total particle volume fraction, fluid viscosity, and volume fraction ratios of each species; see Tables 1–3 for lists of performed simulations. Typically 8–12 independent realizations of each flow situation were performed to obtain good statistical averages of the fluid-particle drag on each particle type in the mixture for chosen Re_1 and Re_2 values.

Strictly speaking, the linear and angular velocities and positions of all the particles will change as the fluid flow evolves, and they should be updated by invoking Newton's laws. It is then not possible to maintain a specified relative velocity (in a local average sense) between the two particle types, as it will also evolve in time. This consideration led us to the so-called *frozen* particle simulations, where the particles were given specified velocities, and the positions and velocities were not updated in time. Such an approach is justifiable in Stokes flow,⁸ but is only an approximation when fluid inertia is significant. Frozen particle simulations are attractive for several reasons:

(a) Freely evolving sedimentation of high-Stokes-number suspensions are inherently unstable and form inhomogeneous microstructure.^{6,28,29} Figure 3 illustrates the formation of inhomogeneous, time-dependent microstructure in a freely evolving ternary suspension simulation. The areas of dark shading indicate areas high in volume fraction while lighter shading indicates regions of lower volume fraction. (We observed such inhomogeneous structures in simulations involving sedimentation of monodisperse and bidisperse suspensions as well. Thus, the origin of these structures is not polydispersity, although polydispersity can certainly be expected to affect the details.)

(b) In some freely evolving simulations where the relative velocity between the different particle phases is large, the

Table 1. List of Bidisperse Suspension Simulations Performed at a Total Volume Fraction of $\phi = 0.2$

N_1	N_2	$\frac{d_2}{d_1}$	ϕ_1	ϕ_2	Re_1	Re_{21}	δ	f_{D1}^*	f_{D2}^*
763	763	1.00	0.10	0.10	1.16	0.50	-1	7.96	3.12
763	763	1.00	0.10	0.10	2.31	1.00	-1	15.98	6.28
763	763	1.00	0.10	0.10	5.78	2.50	-1	40.76	16.21
763	763	1.00	0.10	0.10	11.55	5.00	-1	94.94	43.86
763	763	1.00	0.10	0.10	1.00	2.00	-1	9.66	-9.65
763	763	1.00	0.10	0.10	2.00	4.00	-1	19.35	-19.32
763	763	1.00	0.10	0.10	5.00	10.00	-1	49.12	-49.11
763	763	1.00	0.10	0.10	10.00	20.00	-1	101.23	-101.08
175	175	1.00	0.10	0.10	26.62	13.33	-1	269.96	68.97
175	175	1.00	0.10	0.10	22.79	5.67	-1	206.12	120.83
175	175	1.00	0.10	0.10	56.97	14.16	-1	824.59	565.40
95	36	2.00	0.05	0.15	35.34	13.74	1	290.24	689.42
191	24	2.00	0.10	0.10	2.45	1.87	1	22.30	22.13
191	24	2.00	0.10	0.10	28.86	12.42	1	358.72	295.77
191	24	2.00	0.10	0.10	13.34	5.32	1	135.11	98.66
186	36	2.50	0.05	0.15	5.12	3.70	1	33.36	72.89
382	24	2.50	0.10	0.10	4.38	3.32	1	43.08	37.48
382	24	2.50	0.10	0.10	14.99	19.21	1	7.96	3.12

N_i , d_j/d_i , ϕ_i , Re_i , Re_{ij} , $\delta = \text{sgn}(\Delta U_j - \Delta U_i)$, and f_{Di}^* represent the particle number, diameter ratio, volume fraction, Reynolds number of particles of type i , Reynolds number based on the magnitude of the relative velocity between particles of type j and i , the sign of the relative velocity between particles of type j and i , and the dimensionless fluid-particle drag force experienced by a particle of type i , respectively, in the simulation domain. The fluctuation velocities were zero in all the simulations.

different types of particles tend to segregate. Extracting data on drag force from simulations with such inhomogeneities is very difficult, as the local average volume fractions and local relative velocities in any selected region within the periodic domain are all changing with time.

Frozen particle simulations suppress such inhomogeneities and allow us to compute fluid-particle drag in homogeneous mixtures.

To test the adequacy of frozen particle simulation technique for moderate-Reynolds-number suspensions, we

Table 2. List of Bidisperse Suspension Simulations Performed at a Total Volume Fraction of $\phi = 0.3$

N_1	N_2	$\frac{d_2}{d_1}$	ϕ_1	ϕ_2	Re_1	Re_{21}	δ	f_{D1}^*	f_{D2}^*
1144	1144	1.00	0.15	0.15	1.26	0.50	-1	20.07	8.18
1144	1144	1.00	0.15	0.15	2.52	1.00	-1	40.23	16.43
1144	1144	1.00	0.15	0.15	6.30	2.50	-1	102.05	42.07
1144	1144	1.00	0.15	0.15	12.61	5.00	-1	211.85	89.09
1144	1144	1.00	0.15	0.15	1.09	0.67	-1	22.52	-13.09
1144	1144	1.00	0.15	0.15	2.17	1.35	-1	45.08	-26.18
1144	1144	1.00	0.15	0.15	5.43	3.37	-1	113.51	-65.52
1144	1144	1.00	0.15	0.15	1.00	2.00	-1	23.75	-23.72
1144	1144	1.00	0.15	0.15	2.00	4.00	-1	47.54	-47.50
1144	1144	1.00	0.15	0.15	5.00	10.00	-1	119.71	-119.58
1144	1144	1.00	0.15	0.15	10.00	20.00	-1	244.87	-244.54
1144	1144	1.00	0.08	0.23	0.96	0.41	-1	12.11	-16.82
1144	1144	1.00	0.08	0.23	1.91	0.83	-1	24.24	-33.65
1144	1144	1.00	0.08	0.23	4.78	2.07	-1	60.93	-84.38
1144	1144	1.00	0.08	0.23	9.57	4.13	-1	123.89	-170.51
1144	1144	1.00	0.08	0.23	0.83	0.35	1	13.02	-31.84
1144	1144	1.00	0.08	0.23	1.65	0.69	1	26.05	-63.81
1144	1144	1.00	0.08	0.23	4.13	1.74	1	65.42	-161.51
1144	1144	1.00	0.08	0.23	8.26	3.47	1	132.66	-334.59
1144	1144	1.00	0.08	0.23	1.22	0.50	-1	10.31	13.22
1144	1144	1.00	0.08	0.23	2.43	1.00	-1	20.65	26.50
1144	1144	1.00	0.08	0.23	6.09	2.50	-1	52.17	67.25
1144	1144	1.00	0.08	0.23	12.17	5.00	-1	107.34	139.68
261	261	1.00	0.15	0.15	13.32	6.69	-1	238.35	58.69
261	261	1.00	0.15	0.15	11.40	2.83	-1	187.06	106.56
261	261	1.00	0.15	0.15	22.80	5.67	-1	424.40	249.74
261	261	1.00	0.15	0.15	45.60	2.75	-1	1124.20	980.51
261	261	1.00	0.15	0.15	26.63	13.37	-1	545.12	143.36
287	36	2.00	0.07	0.23	31.41	10.57	1	452.82	1131.90
287	36	2.00	0.15	0.15	15.05	9.41	-1	357.20	18.60
287	36	2.00	0.15	0.15	22.46	13.00	1	522.72	495.49
287	36	2.00	0.15	0.15	4.29	4.00	1	73.97	100.50
287	54	2.50	0.08	0.23	6.03	3.68	1	69.56	182.89
574	36	2.50	0.15	0.15	17.91	19.20	1	307.35	602.51
574	36	2.50	0.15	0.15	5.08	3.32	1	81.40	106.01

See Table 1 for definition of symbols.

Table 3. List of Bidisperse Suspension Simulations Performed at a Total Volume Fraction of $\phi = 0.4$

N_1	N_2	$\frac{d_2}{d_1}$	ϕ_1	ϕ_2	Re_1	Re_{21}	δ	f_{D1}^*	f_{D2}^*
1526	1526	1.00	0.20	0.20	1.39	0.50	-1	45.54	19.21
1526	1526	1.00	0.20	0.20	6.97	2.50	-1	230.66	98.07
1526	1526	1.00	0.20	0.20	13.94	5.00	-1	475.01	205.31
1526	1526	1.00	0.20	0.20	1.13	0.76	-1	50.24	-28.64
1526	1526	1.00	0.20	0.20	2.26	1.53	-1	100.55	-57.29
1526	1526	1.00	0.20	0.20	5.66	3.81	-1	252.63	-143.35
1526	1526	1.00	0.20	0.20	11.31	7.63	-1	513.37	-287.58
1526	1526	1.00	0.20	0.20	1.00	2.00	-1	52.59	-52.57
1526	1526	1.00	0.20	0.20	2.00	4.00	-1	105.27	-105.21
1526	1526	1.00	0.20	0.20	5.00	10.00	-1	264.49	-264.35
1526	1526	1.00	0.20	0.20	10.00	20.00	-1	537.42	-537.16
1526	1526	1.00	0.20	0.20	56.98	14.16	-1	2958.50	1500.60
1526	1526	1.00	0.20	0.20	26.62	13.33	-1	1095.60	188.30
1526	1526	1.00	0.10	0.30	0.93	0.37	-1	26.33	-37.05
1526	1526	1.00	0.10	0.30	1.87	0.74	-1	52.68	-74.14
1526	1526	1.00	0.10	0.30	4.67	1.84	-1	132.11	-185.82
1526	1526	1.00	0.10	0.30	9.34	3.68	-1	266.95	-374.74
1526	1526	1.00	0.10	0.30	0.74	0.53	-1	27.89	-70.98
1526	1526	1.00	0.10	0.30	1.47	1.05	-1	55.82	-142.17
1526	1526	1.00	0.10	0.30	3.68	2.63	-1	139.98	-358.78
1526	1526	1.00	0.10	0.30	7.37	5.26	-1	282.54	-737.08
1526	1526	1.00	0.10	0.30	1.33	0.50	-1	23.20	30.75
1526	1526	1.00	0.10	0.30	2.66	1.00	-1	46.46	61.61
1526	1526	1.00	0.10	0.30	6.64	2.50	-1	117.08	155.72
1526	1526	1.00	0.10	0.30	13.29	5.00	-1	239.34	320.85
191	72	2.00	0.10	0.30	33.50	9.61	1	822.50	2227.80
382	48	2.00	0.20	0.20	11.39	6.48	1	357.27	483.58
382	48	2.00	0.20	0.20	33.39	18.68	1	1327.50	1750.80
382	48	2.00	0.20	0.20	6.68	3.74	1	209.30	275.27
382	72	2.50	0.10	0.30	7.27	3.68	1	156.08	436.63
764	48	2.50	0.20	0.20	5.95	3.32	1	198.29	231.38
764	48	2.50	0.20	0.20	21.44	19.21	1	771.13	1285.10

See Table 1 for definition of symbols.

compared the fluid-particle drag results obtained from frozen simulations where the particle positions were not updated in time with those obtained from simulations where the particles were allowed to move but treated as elastic granular gas (as in Wylie et al.²⁰), (i.e., the particles do not respond to fluid-particle drag, but execute elastic collisions). In these test simulations, all the particles were of the same size and computations were done at various grid resolutions. Both types of simulations had the same Re_m , Re_T , and particle volume fraction. The hydraulic radius of the interstitial region is given by,

$$r_h = \frac{\langle d \rangle (1 - \phi)}{6\phi}. \quad (18)$$

As resolution increases, the particle diameter-to-lattice spacing ratio, d , and the hydraulic radius-to-lattice spacing ratio, r_h , increase. In Figure 4, we have plotted the fluid-particle drag obtained from both granular gas and frozen simulations as a function of r_h^{-2} for two different combinations of Re_m and Re_T . It is clear that the two approaches yield different estimates for the fluid-particle drag force at any finite grid resolution; this difference decreases as the value of r_h^{-2} decreases (which is equivalent to increasing resolution). It is also clear that the fluid-particle drag varies linearly with r_h^{-2} as already noted by van der Hoef et al.¹² and Beetstra et al.¹⁹; when the fluid-particle drag results are extrapolated to infinite resolution, the difference between frozen and granular gas simulations becomes small. Therefore, in our work we have performed frozen particle simulations at a minimum of two different

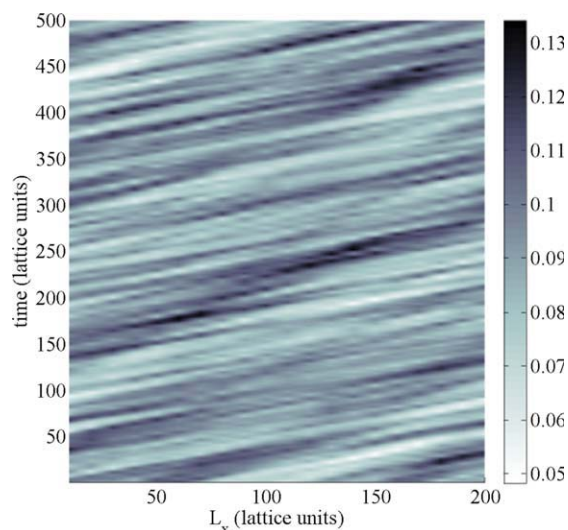


Figure 3. Space-time plot of volume fraction in a freely evolving ternary suspension.

The vertical axis is time, and the horizontal axis is the position in the simulation domain. The variations in the gray scale indicate variations in volume fraction with the darker regions corresponding to regions of higher volume fraction. This simulation was performed in a $200 \times 70 \times 70$ periodic box. The particle diameters used in this simulation were $d_1 = 7.6$, $d_2 = 9.6$, and $d_3 = 11.6$, with respective particle numbers of $N_1 = 56$, $N_2 = 120$, and $N_3 = 24$, giving a total particle volume fraction of $\phi = 0.1$. A gravitational force $g \langle d \rangle^3 / \nu^2 = 1.11 \times 10^{-2}$ is applied in the x-direction, and balanced by a pressure gradient equal to the weight of the suspension per unit volume. [Color figure can be viewed in the online issue, which is available at www.interscience.wiley.com.]

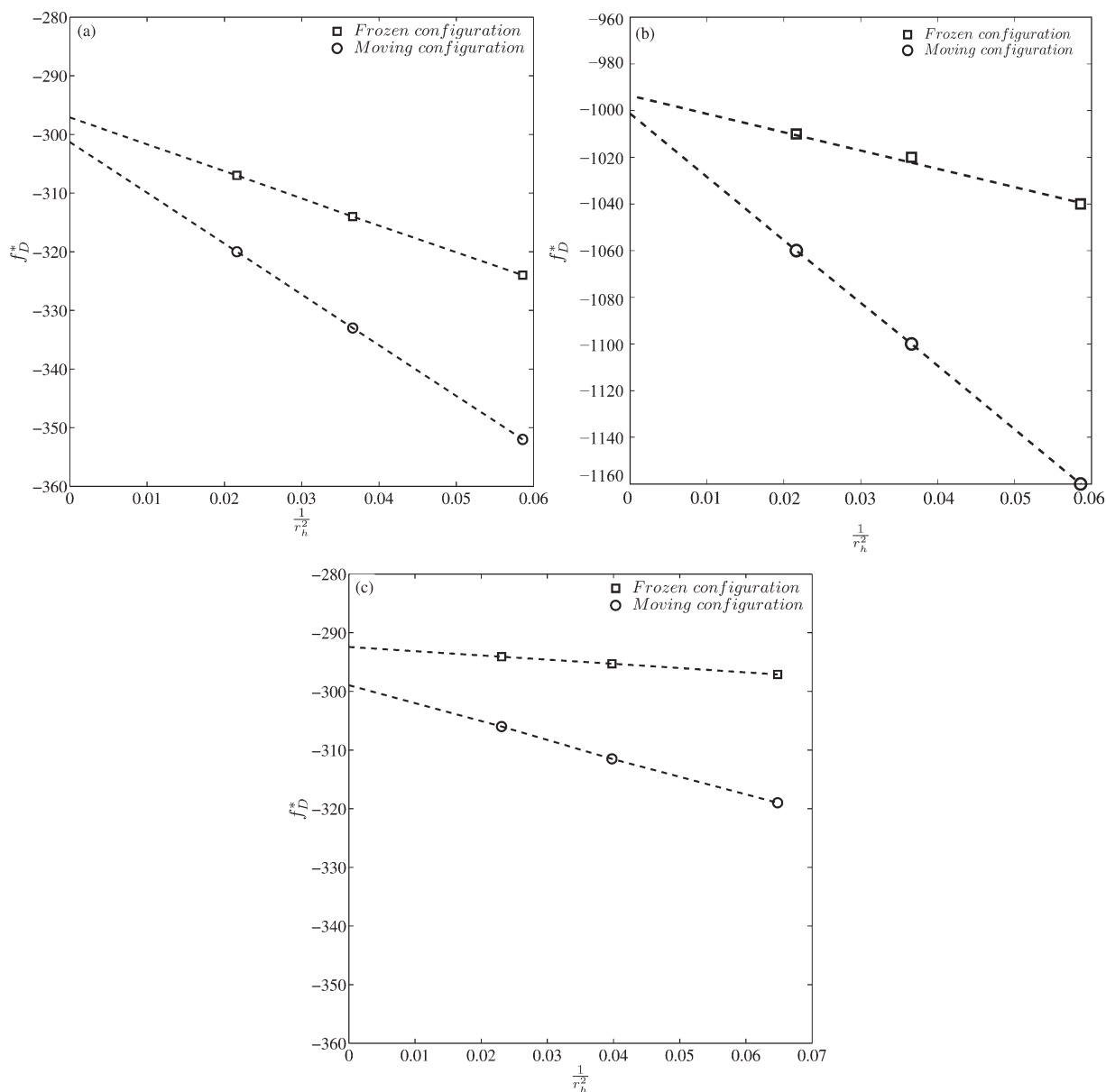


Figure 4. Dimensionless fluid-particle drag force as a function of grid resolution.

Shown are results obtained from frozen particle simulations and those obtained from simulations where the particles were allowed to move as granular gas. All the particles were of the same size. Both types of simulations had the same Re_m , Re_T , and particle volume fraction. (a) $Re_m = 7$, $Re_T = 0.6$; $\mu_f = 0.03$ (lattice units), (b) $Re_m = 20$, $Re_T = 1.2$; $\mu_f = 0.03$ (lattice units), and (c) $Re_m = 7$, $Re_T = 0.6$; $\mu_f = 0.36$ (lattice units).

resolutions and extrapolated the fluid-particle drag to the infinite resolution case using a linear fit as illustrated in Figure 4. At higher fluid viscosities like $\mu_f = 0.36$, we have found that extrapolation of the fluid-particle drag results is unnecessary. It can be seen in Figure 4c that while the fluid-particle drag at any finite resolution differs between frozen and moving simulations, the fluid-particle drag results indeed approach one another in the limit of infinite resolution. Furthermore, if one focuses on the dependence of the fluid-particle drag from the *frozen* simulation case in Figure 4c (for a higher lattice viscosity) as a function of r_h^{-2} it can be seen that the fluid-particle drag changes by about 1.6% from the lowest resolution case to the extrapolated fluid-particle drag. Because

of the decreased dependence of the fluid-particle drag on grid resolution at higher fluid viscosities, the drag results given at $\mu_f = 0.36$ were not extrapolated in an attempt to decrease the computational demand of the study.

Frozen Particle Simulation Results

Tables 1–3 give a list of the simulations performed at each volume fraction in this work. The fluctuation velocities of the particles were set to zero. The total force acting on the two types of particles and the pressure gradient required to maintain the average fluid velocity at zero were extracted from the simulations. The fluid-particle drag force on the

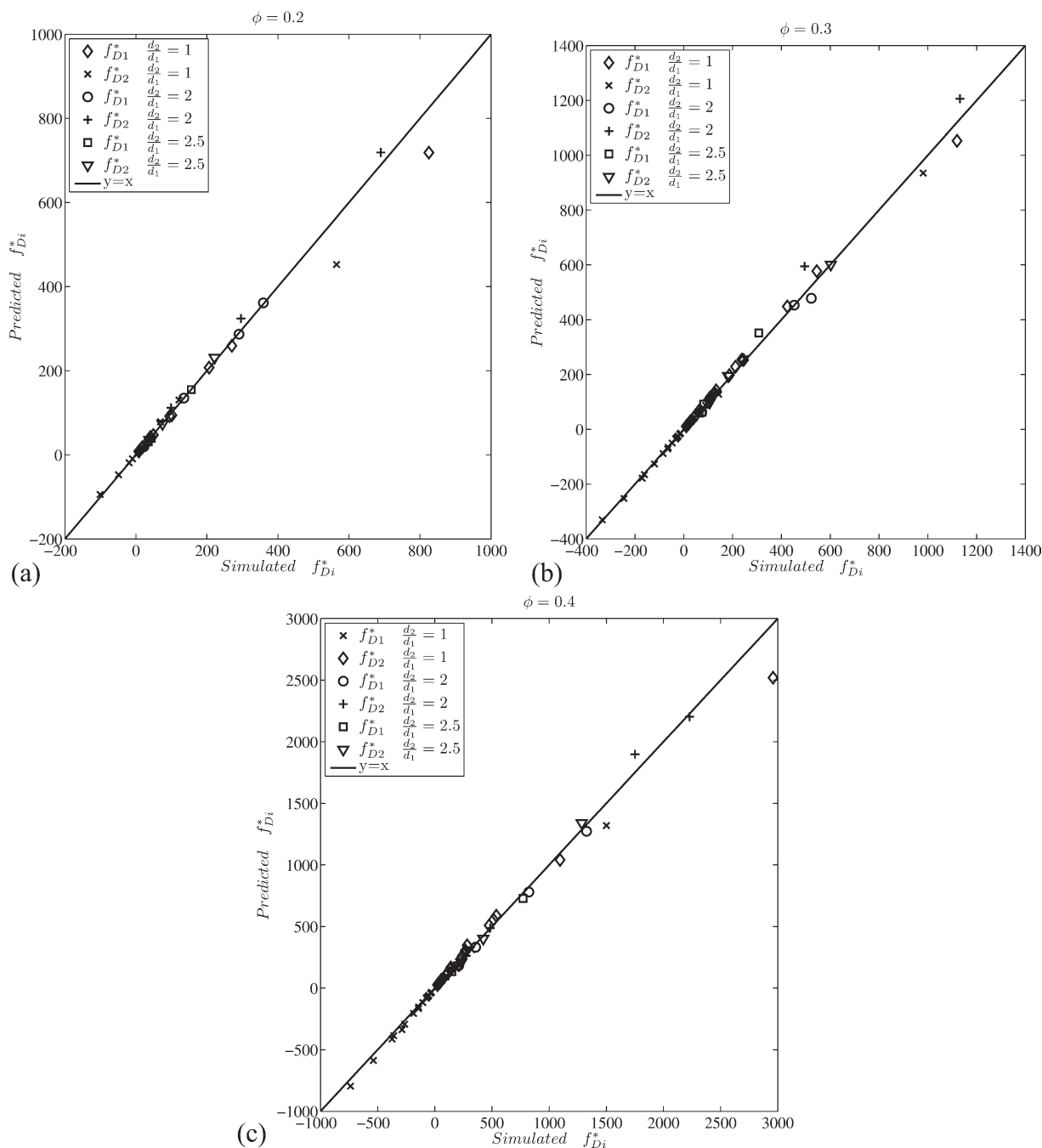


Figure 5. Parity plots showing the simulated fluid-particle drag force and that predicted by the proposed drag force model for bidisperse systems with different particle sizes, volume fraction ratios and Reynolds numbers summarized in Tables 1–3.

Results are shown for three different total volume fractions: (a) $\phi = 0.2$, (b) $\phi = 0.3$, (c) $\phi = 0.4$.

two particle types was then found using Eq. 10a and made dimensionless using the following relationship: $f_{Di}^* = \rho_f (d_i)^3 f_{Di} / \mu_f^2$. These drag results were then compared with values found from the drag force model given by Eqs. 2–4, 6, and 11–17. Figures 5a–c show parity plots comparing the model with simulation data; the proposed model fits the data reasonably well with an average deviation between model and simulation being about 5%, while the maximum deviations were about 25%.

To demonstrate that our proposed fluid-particle drag relation can be generalized to polydisperse mixtures of spheres with nonzero particle–particle relative motions, we performed two ternary suspension simulations at $\phi = 0.21$ and $\phi = 0.3$. Table 4 gives the ternary fluid-particle drag results obtained from lattice-Boltzmann simulations with the predicted fluid-particle drag obtained from Eqs. 2–4, 6, and 11–17. It can be seen that the proposed model captures the

Table 4. List of Ternary Suspension Results at $\phi = 0.21$ and $\phi = 0.3$

	$\phi = 0.21$	$\phi = 0.3$
$\phi_1/\phi_2/\phi_3$	0.07/0.07/0.07	0.10/0.10/0.10
$d_1/d_2/d_3$	14.0/17.5/35.0	14.0/17.5/35.0
$N_1/N_2/N_3$	261/134/17	373/191/24
$\langle d \rangle$	19/1	19.1
$Re_1/Re_2/Re_3$	6.8/9.1/28.3	8.3/10.6/29.9
$f_{D1}^*/f_{D2}^*/f_{D3}^*$ (simulation)	30.2/48.4/128.1	81.9/105.7/269.3
$f_{D1}^*/f_{D2}^*/f_{D3}^*$ (proposed model)	31.5/41.9/130.2	60.5/83.7/294.4

See Table 1 caption for definition of symbols.

fluid-particle drag results of the ternary suspension simulations with an average deviation of 12.5%.

Figure 6 illustrates that the fluid-mediated (hydrodynamic) particle-particle drag (namely, the second term on the right hand side of Eq. 11) accounts for 0–30% of the fluid-particle drag force in a bidisperse suspension depending on the magnitude of the relative velocity between particle species. From Figure 6, it can be seen that the importance of the fluid-mediated particle-particle drag increases as particle diameter ratio is increased, leading to the conclusion that increases in particle diameter ratio for a fixed Re_{mix} and Re_{12} increases the contribution of the fluid-mediated particle-particle drag to the total fluid-particle drag experienced by a particle of a given type.

The fluid-mediated particle-particle drag force can be compared with the particle-particle drag that results from direct collisions between particles of different types, for which Syamlal³⁰ proposed the following:

$$f_{i-j}^* = -6\phi_i\phi_jg_0Re_{ij}^2\text{sgn}(\Delta U_i - \Delta U_j) \left(\frac{\left(\frac{\rho_i}{\rho_f}\right)\left(\frac{\rho_j}{\rho_f}\right)}{\frac{\rho_i}{\rho_f} + \frac{\rho_j}{\rho_f}} \right) \quad (19)$$

where g_0 is the radial distribution function (for the ij pair) at contact for a polydisperse hard sphere mixture. This leads to:

$$\frac{f_{D-i-j}^*}{f_{i-j}^*} = \frac{6\alpha(1-\phi)(F_{Di-fixed}^*F_{Dj-fixed}^*)}{g_0Re_{ij}(F_{Di-fixed}^* + F_{Dj-fixed}^*)} \left(\frac{\left(\frac{\rho_i}{\rho_f}\right) + \left(\frac{\rho_j}{\rho_f}\right)}{\left(\frac{\rho_i}{\rho_f}\right)\left(\frac{\rho_j}{\rho_f}\right)} \right). \quad (20)$$

Since $\frac{F_{Di-fixed}^*F_{Dj-fixed}^*}{F_{Di-fixed}^* + F_{Dj-fixed}^*}$ is only weakly dependent on Reynolds number, the most significant dependence on Reynolds number comes through Re_{ij} , and therefore as the difference between the Reynolds numbers of different particle species increases, the collisional particle-particle drag dominates the fluid-mediated particle drag term. The quantitative analysis of Yin and Sundaresan⁷ about the relative importance of the fluid-mediated particle-particle drag and that due to collisions in the Stokes flow regime remains largely unchanged even in the presence of moderate inertia.

Summary

In this study, we combine the fluid-particle drag relation described by Yin and Sundaresan^{7,8} for low Reynolds number flows and that for fixed beds under moderate fluid inertia given by Beetstra et al.¹⁹ and construct a drag force model that applies to polydisperse, high-Stokes-number, and moder-

ate-Reynolds-number suspensions of spherical particles, where the local average velocities of particles of different types are not the same. The proposed fluid-particle drag force model is summarized by Eqs. 2–4, 6, 11–17.

To test this model, a number of lattice-Boltzmann simulations of fluid flow in polydisperse assemblies of particles were carried out from which computational data on fluid-particle drag were gathered. The particle mixture Reynolds number was varied from $0 \leq Re_{mix} \leq 40$, over a particle volume fraction range of $0.2 \leq \phi \leq 0.4$, with volume fraction ratios of $1 \leq \phi_i/\phi_j \leq 3$, and particle diameter ratios varying from $1 \leq d_i/d_j \leq 2.5$. Within this parameter range, the proposed fluid-particle drag relation predicts the fluid-particle drag in bidisperse and ternary systems with an average deviation of 5% and 12.5%, respectively.

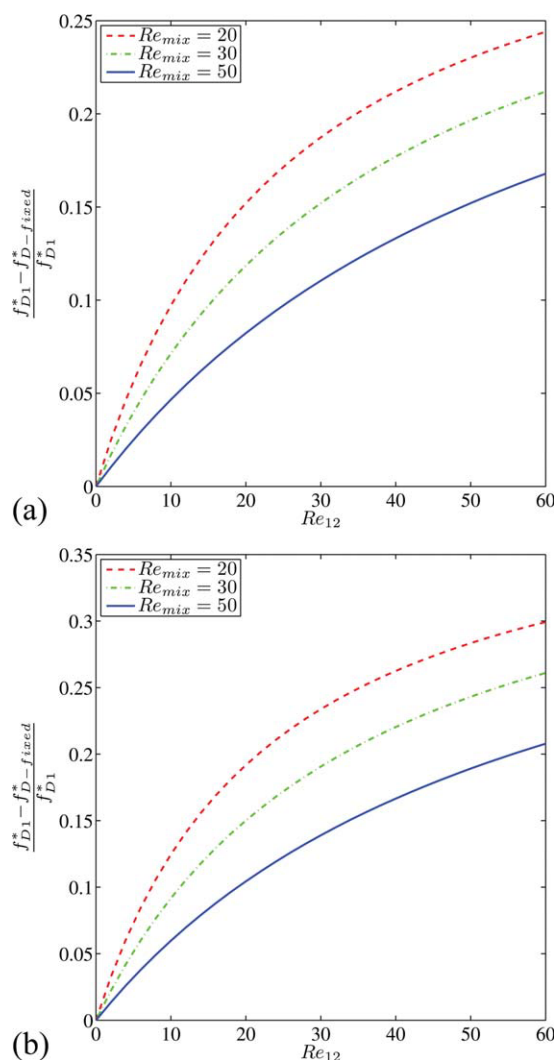


Figure 6. The fluid-mediated particle-particle drag force (normalized with the total fluid-particle drag force) as a function of Re_{12} for the proposed fluid-particle drag relation at two different diameter ratios: (a) $d_1:d_2 = 1$, (b) $d_1:d_2 = 2$.

[Color figure can be viewed in the online issue, which is available at www.interscience.wiley.com.]

Acknowledgments

This research was supported by, US Department of Energy (DE-FC26-07NT43098), ExxonMobil Research and Engineering Co. and ACS Petroleum Research Fund (43901-AC9).

Literature Cited

1. Fan LS, Zhu C. *Principles of Gas-Solids Flows*. New York: Cambridge University Press, 1998.
2. Jackson R. *The Dynamics of Fluidized Particles*. Cambridge: Cambridge University Press, 2000.
3. Gidaspow D. *Multiphase Flow and Fluidization: Continuum and Kinetic Theory Descriptions*. London: Academic Press, 1994.
4. Sangani A, Koch D. Particle pressure and marginal stability limits for a homogeneous monodisperse gas-fluidized bed: kinetic theory and numerical simulations. *J Fluid Mech.* 1999;400:229–263.
5. Ten Cate A, Sundaresan S. Analysis of unsteady forces in ordered arrays of monodisperse spheres. *J Fluid Mech.* 2006;552:257–287.
6. Derksen JJ, Sundaresan S. Direct numerical simulations of dense suspensions: wave instabilities in fluidized beds. *J Fluid Mech.* 2007;587:303–336.
7. Yin X, Sundaresan S. Drag Law for Bidisperse Gas-Solid suspensions Containing Equally Sized Spheres. *Ind Eng Chem Res.* 2009;48:227–241.
8. Yin X, Sundaresan S. Fluid-particle drag in low-Reynolds-number polydisperse gas-solid suspensions. *AIChE J.* 2009;55:1352–1368.
9. Richardson JF, Zaki WN. The sedimentation of a suspension of uniform spheres under conditions of viscous flow. *Chem Eng Sci.* 1954;3:65–73.
10. Wen CY, Yu YH. Mechanics of fluidization. *Chem Eng Prog Symp Ser.* 1966;62:100–111.
11. Benyahia S, Syamlal M, O'Brien TJ. Extension of Hill-Koch-Ladd drag correlation over all ranges of Reynolds number and solids volume fraction. *Powder Technol.* 2006;162:166–174.
12. van der Hoef MA, Beetstra R, Kuipers JAM. Lattice-Boltzmann simulations of low-Reynolds-number flow past mono- and bidisperse arrays of spheres: results for permeability and drag force. *J Fluid Mech.* 2005;528:233–254.
13. Di Felice R. The voidage function for fluid-particle interaction systems. *Int J Multiphase Flow.* 1994;20:153–159.
14. Mazzei L, Lettieri P. A drag force closure for uniformly dispersed fluidized suspensions. *Chem Eng Sci.* 2007;62:6129–6142.
15. Geldart D, Baeyens J, Pope DJ, Van De Wijer P. Segregation in beds of large particles at high velocities. *Powder Technol.* 1981;30:195–205.
16. Joseph GG, Leboireiro J, Hrenya CM, Stevens AR. Experimental segregation profiles in bubbling gas-fluidized beds. *AIChE J.* 2007;53:2804–2813.
17. Hoffman AC, Janssen LPBM, Prins J. Particle segregation in fluidized binary mixtures. *Chem Eng Sci.* 1993;48:1583–1592.
18. Rowe PN, Nienow AW. Particle mixing and segregations in gas fluidized beds: a review. *Powder Technol.* 1976;15:141–147.
19. Beetstra R, Van Der Hoef MA, Kuipers JAM. Drag force of intermediate Reynolds number flow past mono- and bidisperse arrays of spheres. *AIChE J.* 2007;53:489–501.
20. Wylie JJ, Koch DL, Ladd AJC. Rheology of suspensions with high particle inertia and moderate fluid inertia. *J Fluid Mech.* 2003;480:95–118.
21. Beetstra R, van der Hoef MA, Kuipers JAM. Erratum. *AIChE J.* 2007;53:3020.
22. Ladd AJC. Numerical simulations of particulate suspensions via a discretized Boltzmann equation. Part 1. Theoretical foundation. *J Fluid Mech.* 1994;271:285–309.
23. Ladd AJC. Numerical simulations of particulate suspensions via a discretized Boltzmann equation. Part 2. Numerical results. *J Fluid Mech.* 1994;271:311–339.
24. Ladd AJC, Verberg R. Lattice-Boltzmann simulations of particle-fluid suspensions. *J Stat Phys.* 2001;104:1191–1251.
25. Hill R, Koch DL, Ladd AJC. The first effects of fluid inertia on flows in ordered and random arrays of spheres. *J Fluid Mech.* 2001;448:243–278.
26. Hill R, Koch DL, Ladd A. Moderate-Reynolds-number flows in ordered and random arrays of spheres. *J Fluid Mech.* 2001;448:243–278.
27. Nguyen N-Q, Ladd AJC. Lubrication corrections for lattice-Boltzmann simulations of particle suspensions. *Phys Rev E.* 2002;66:046708.
28. Valiveti P, Koch DL. The inhomogeneous structure of a bidisperse sedimenting gas-solid suspension. *Phys Fluids.* 1999;11:3283–3305.
29. Sundaresan S. Instabilities in fluidized beds. *Annu Rev Fluid Mech.* 2003;35:63–88.
30. Syamlal M. The particle-particle drag term in a multiparticle model of fluidization. Technical Report DOE/MC/21353-2373. US Department of Energy, NTIS/DE87006500, Washington D.C., 1987.

Manuscript received Aug. 24, 2009, and revision received Oct. 22, 2009, and final revision received Oct. 28, 2009.